

MICROSTRUCTURAL EFFECTS ON THE BRITTLINESS OF HIGH STRENGTH CONCRETES

C.Taşdemir and M.A.Taşdemir
Faculty of Civil Engineering, Istanbul Technical University,
Istanbul, Turkey
R.Grimm and G.König
Institut für Massivbau, Technische Hochschule Darmstadt,
Darmstadt, Germany

Abstract

The influence of silica fume and coarse aggregate size on the strain localization, post-peak softening response and brittleness of high strength concretes was investigated. Uniaxial tension tests were performed using a closed-loop electro-hydraulic loading system. Based on the mechanical test results and scanning electron microscopic examination of the aggregate-paste interfacial zone, it is conjectured that in concretes which contain silica fume, the cracks usually are transgranular, i.e., they travel through the aggregates; the interfacial zone for these concretes are stronger and more homogeneous, and the fracture occurs in more brittle manner. However, in concretes without silica fume the cracks usually develop around the coarse aggregates resulting in an inter-coarse aggregate type of fracture.

1 Introduction

In microstructural terms, normal concrete is a complex system of solid phases, pores and water, with a high degree of heterogeneity. This

heterogeneity can be considered on several levels. For material modelling purposes Wittmann (1983) introduced the idea of three levels, such as micro, meso and macro-levels. To establish a realistic failure model at the macro-level, an insight into the fracture mechanisms at the meso-level is required. However, at the meso-level, the heterogeneity results in a non-uniform internal strain distribution within the concrete composite. Since the interface between the aggregates and cement paste is the weakest link, the mechanical behaviour of concrete is significantly affected by the properties of interfacial zone, especially, the fracture of concrete is very sensitive to the properties of this zone (Bentur 1991, Sarkar 1994). The interface failure may be considered at meso-level. The development of bond crack at the aggregate-matrix interfaces plays an important role in the inelastic behaviour of concrete. A considerable portion of the total strain is concentrated at interfaces and the final failure occurs in mortar, bridging bond cracks. Recent advances show that there are two principal aspects of interfaces in cement and concrete: 1°) the microstructural features of the interfacial regions, including their effects on concrete properties; and 2°) models of the interface effects on the properties of concrete through the application of continuum and fracture mechanics approaches (Shah 1990, Gettu et al. 1991, Mitsui et al. 1994, Taşdemir et al. 1994, 1995).

Addition of silica fume into the concrete, because of its ultrafine size and spherical shape leads to important changes in fresh concrete. It also affects the pore size distribution, the mechanical properties and durability of concrete. The concept of the new CEB-FIP Model Code 1990 indicates BS 80 as the highest quality concrete class, which implies the cube compressive strength of about 100 MPa (Walraven 1991). However, the use of silica fume in concrete has changed this situation, in some countries, concrete with a cube strength of 120 MPa is now readily available as pumping concrete (König et al. 1993).

There is a growing interest in the study of aggregate-matrix interfaces in concrete. Previous studies on the fracture and microstructure of this region in normal strength concrete has led to some useful information, however, more research and quantitative measurements are needed for a better understanding of the fracture process in HSCs with and without silica fume. In particular, a more realistic approach is required to investigate real concrete behaviour instead of mortar containing model aggregate (Taşdemir et al. 1994, 1995).

The aim of this work is to investigate, the influence of silica fume addition and aggregate particle size on the brittleness of HSCs subjected to uniaxial tension. The investigations were supported with microstructural studies at the aggregate-paste interfacial zone for corresponding specimens by using scanning electron microscope (SEM) and Energy Dispersive X-Ray Analyzer (EDX).

2 Experimental program

As shown in Table 1, four different HSC mixes at constant water/cement (or water/cement+silica fume) ratio were prepared by using the same cement (PZ 45) and natural sand. Two different sizes of gravel aggregate were chosen either 4-8mm or 8-16mm in the study. For each maximum aggregate size, two different concretes; one with and one without silica fume were cast. The silica fume content was chosen as 10 percent by weight of the cement. The water/binder ratio was kept at 0.30 in all the four concretes and a sodium naphthalene sulfonate type superplasticizer was used in all the mixes. Adjusting the admixture dosage, about the same nominal spread (43 cm to 48 cm) was maintained. Concretes without and with silica fume were coded as NC and SC, respectively. The number following NC and SC shows the maximum aggregate size. The mix proportions and properties of fresh concretes are given in Table 1. The specimens were cured in lime saturated water, for 56 days and afterwards, stored in a room maintained at $20\pm 2^{\circ}\text{C}$ and $65\pm 5\%$ relative humidity until the time of tests, that is 72 days after the specimens casting.

Table 1. Mix proportions of concretes with and without silica fume

Mix Code		NC8	SC8	NC16	SC16
Cement, C (kg/m^3)		405	372	408	373
Silica fume, SF(kg/m^3)		0	38	0	38
Sand (kg/m^3)	0-1 mm	370	374	373	375
	0-2 mm	370	374	373	375
Coarse aggregate (kg/m^3)	4-8 mm	1109	1122	-	-
	8-16 mm	-	-	1117	1125
Superplasticizer (kg/m^3)		16.2	16.4	13.2	13.3
Water, W (kg/m^3)		122	123	123	123
W / (C+SF)		0.30	0.30	0.30	0.30
SF / C		0	0.10	0	0.10
Air content (%)		2.0	1.0	1.6	1.0
Spread (cm)		43	45	46	48
Density of Fresh Concrete (kg/m^3)		2392	2419	2407	2422

At least three specimens of each concrete mix were tested under each type of loading at 72 days. For the uniaxial tension tests, a panel of 400mm×300mm×100mm, for obtaining the complete stress-strain curve in compression and modulus of elasticity, cylinder specimens with a diameter of 100mm and height of 200mm, were prepared. For the standard compressive tests, four 100mm cubes, and for the splitting tests, cylinder specimens were cast.

3 Test procedure

The uniaxial tests were carried out on double-edge notched specimens of 250mm×100mm×100mm. They were sawn cut from a 100mm thick panel of 400mm×300mm×100mm. Then, the effective cross-section was reduced to 60mm×100mm by means a saw cut. The specimens were loaded by a Schenck closed-loop universal testing machine with a capacity of 1500 kN. The stiffness of its frame was 9000 MN/m. Longitudinal deformations of the specimen, as shown in the inset in Fig.1, was measured with two LVDTs of 50mm base mounted on the notched sides of the specimen. Specimen ends were fixed to the loading plates of the test machine by using an epoxy-based resin. During the test, load versus deformation was recorded. The details of the test method are given by Rimmel (1992).

The fracture energy, G , is calculated from the following equation:

$$G_F = \int_0^{w_F} \sigma(w) dw \quad (1)$$

This energy is the total energy dissipated on an unit crack surface and is equal to the area under the stress-crack width curve, where w_F is the crack width at failure. In G_F calculations, as shown in the inset in Fig.1, stress-total deformation curves $\sigma - \delta$ were transformed to the stress-crack width $\sigma - w$ curves, where the crack width is defined as the total deformation minus the elastic and residual deformations represented by an unloading line drawn from the top of $\sigma - \delta$ curve parallel to the linear part of the ascending branch. The characteristic length of the material, l_{ch} , is given by the following expression:

$$l_{ch} = \frac{EG_F}{f_t^2} \quad (2)$$

where f_t is the tensile strength.

The complete stress-strain curves were also obtained using the same closed-loop testing machine mentioned above. The static modulus of

elasticity was calculated from the ascending part of stress-strain curve for stresses below approximately 33% of the ultimate strength. The splitting tensile strengths were determined on cylinder specimens with a diameter of 150mm and height of 150mm. Table 2 summarises the test results obtained for the four concretes tested in this investigation.

Table 2. Properties of hardened concrete

Mix code	NC8	SC8	NC16	SC16
Cube compressive strength, MPa	78.3	101.9	81.5	107.8
Cylinder compressive strength, MPa	57.2	80.0	62.2	83.0
Splitting tensile strength, MPa	3.79	4.45	4.44	5.29
Modulus of Elasticity (E), GPa	40.0	45.2	42.7	47.3
Fracture energy (G), N/m	64	70	95	104
Tensile strength (f_t), MPa	3.24	4.00	3.78	4.32
Characteristic length l_{ch} , mm.	238	198	284	264
Total deformation at failure, mm.	0.154	0.155	0.240	0.180

4 Results and discussions

As shown in Table 2, there is significant effect of silica fume replacement on compressive strength values. In concretes with silica fume, the increase in compressive strength is 30% higher than that of non-silica fume ones. The mechanical test results are evaluated below by combining microstructural investigations at the aggregate-matrix interfaces.

4.1 The shape of the stress-deformation curve

In concretes without silica fume, when the stress reaches approximately 85% of the tensile strength, the curves deviates from linearity; this is the pre-peak nonlinearity. At this stage, damage starts to increase at the interfaces due to the heterogeneity of the concrete. At peak stress, microcracks begin to localize to form a discrete macroscopic crack. In concrete NC16, as shown in Fig.1, the softening response has a longer tail than that of NC8, due to the aggregate size. It can be concluded that the amount of crack bridging is determined by the maximum size of the aggregates and that a longer tail is an indication of the increased load

energy G_F is strongly dependent on the maximum aggregate size; G_F increases as the aggregate size increases. However the effect of silica fume replacement on both G_F and l_{ch} is not significant. Reason is that the tensile strength values of concretes with silica fume are greater than that of non-silica fume ones, their descending branches are steeper and they have shorter tails. Thus, the replacement of silica fume affects strengths significantly, but, the increase in the fracture energy is not substantial, and these concretes become more brittle.

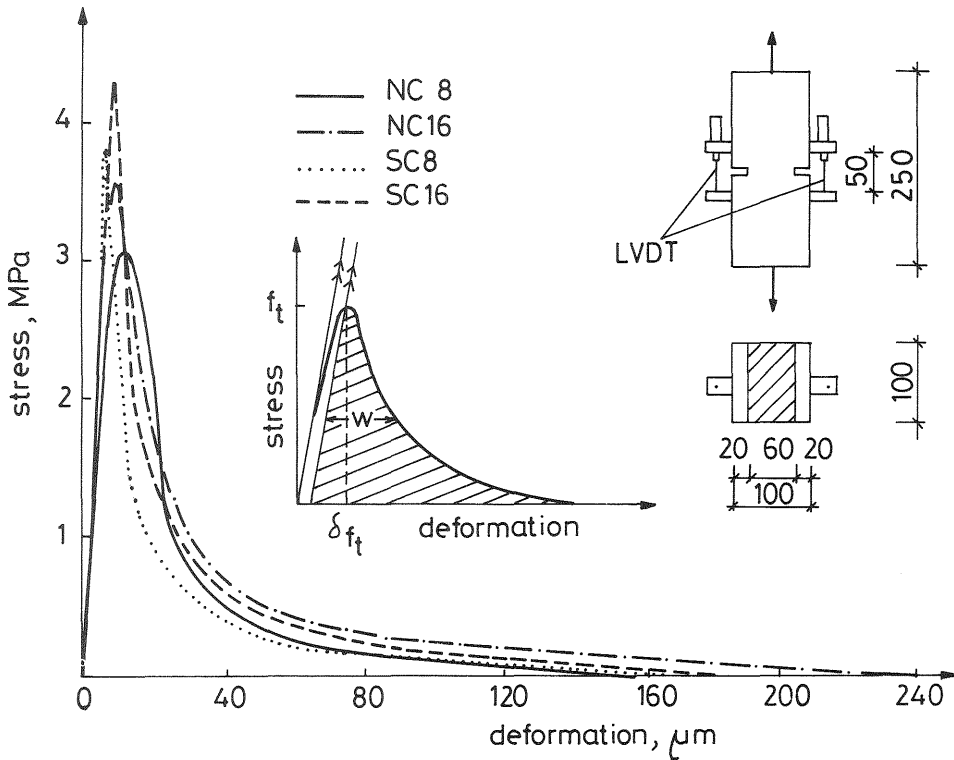


Fig.1. Typical results of stress-deformation curves obtained from uniaxial tension tests. Schematic representation of G_F and the sizes of test specimens are also shown in the inset.

In concretes with silica fume, the ascending branch is almost linear up to approximately 95% of peak stress. After the peak point, stress decreases rapidly with increasing deformation. Concretes with silica fume are more homogeneous, and the difference between interface and mortar strengths decreases. Similar conclusions were made by Taşdemir et al.

strengths decreases. Similar conclusions were made by Taşdemir et al. (1994) for limestone coarse aggregate concretes tested in bending. They reported that in concretes without silica fume both G_F and l_{ch} increase as the aggregate size increases, on the contrary, in the concretes with silica fume, the fracture energy and especially the characteristic length decrease dramatically for both aggregate sizes. However, in this work, for concretes with silica fume, the characteristic length decreases slightly. The type of loading, the type and texture of coarse aggregate may play important roles in the determination of fracture parameters. For the further studies, experimental work should be expanded to study the size effects of test specimens, the effects of the surface texture and mineralogy of the aggregates, curing conditions, age, loading rate and loading conditions.

4.2 Microstructure of the aggregate paste interface

After completion of tension tests the fracture surfaces were examined using both a stereo microscope and a scanning electron microscope (SEM). In concretes with silica fume, the cracks usually traversed through the aggregate; transgranular type of fracture was observed, and it was brittle in nature, in concretes without silica fume, however, the cracks usually developed around the coarse aggregate resulting in an inter-coarse aggregate type of fracture.

In concretes without silica fume, the SEM micrograph in Fig.2, shows a profusion of calcium hydroxide (CH) at the aggregate-paste interface. Not only are the CH crystals massive, often up to 20 μ m in size, they are mostly tabular and oriented. This is a characteristic feature of normal concrete, or concrete without any mineral admixture. Apart from CH, some ettringite (AFt) crystals were also identified in this region. The calcium silicate hydrate (C-S-H) is also much less dense. The paste is also porous and is characterized by the presence of fibrous or Type 1 C-S-H. Ettringite needles and tabular CH crystals are also identifiable in the paste. The air voids are full of platy CH crystals.

In concretes with silica fume (Fig.3), the interfacial zone is composed of dense C-S-H. The air voids and other vacant spaces in this region are empty, and show no deposition of CH, mono-sulphate or ettringite crystals. Dense paste identical to that of the interfacial zone was observed. As in transition zone, the air voids in the paste are empty. The observation of abundant CH crystals at the paste-aggregate interface in the non-silica fume concrete corresponds well with those of others (Skalny 1989, Sarkar 1994 and Taşdemir et al. 1995). The difference in the paste-aggregate interfacial microstructure of silica fume and non-silica fume concrete is attributable to the pozzolanic reaction of silica fume, which consumes the CH normally concentrated in this zone; it is replaced by dense C-S-H.

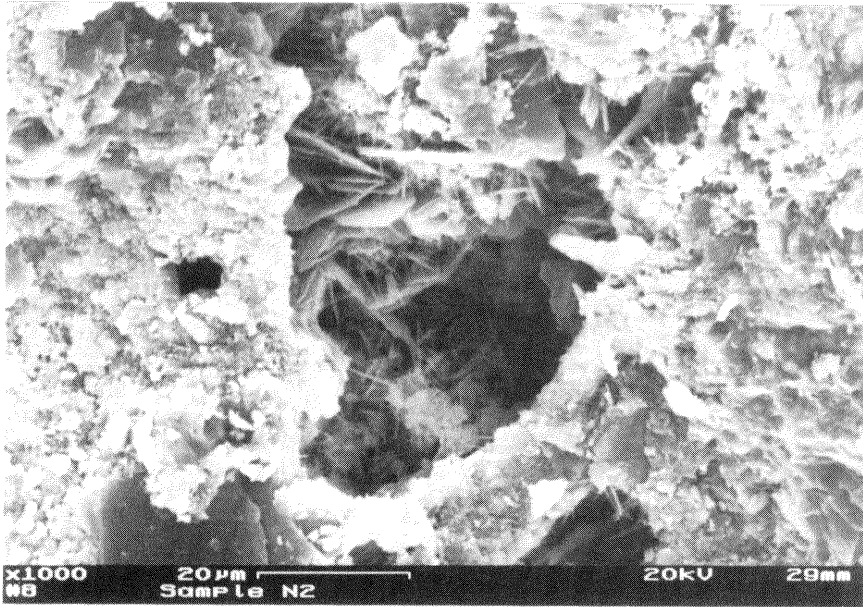


Fig.2. SEM micrograph at the paste-aggregate interface in concretes without silica fume.

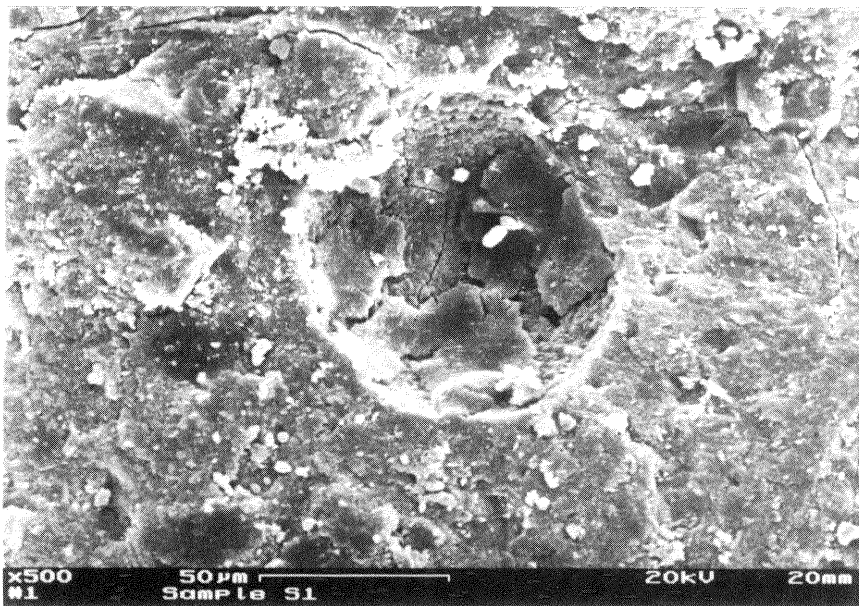


Fig.3. SEM micrograph at the paste-aggregate interface in concretes with silica fume.

5 Conclusions

In the light of mechanical tests, examinations of the fracture surfaces and the microstructural studies of the aggregate-matrix interfaces, the following conclusions can be drawn:

1. In concrete without silica fume, with 16mm maximum size of aggregate the descending branch of the load-deformation curves decreases more slowly and a longer tail is observed. However, in the concrete with silica fume, a steeper gradient of the softening branch with a shorter tail is observed.
2. In concrete without silica fume, the fracture energy strongly depends on the maximum size of aggregate, it increases as the aggregate size increases. However, the characteristic length slightly increases with the aggregate size. In concretes with silica fume, the fracture energy is slightly higher than that of non-silica fume ones due to their high tensile strength values, however, the characteristic length slightly decreases due to their brittleness.
3. Based on the fracture tests and microscopic studies at the aggregate matrix interface, it can be concluded that in concretes which contain silica fume, the cracks usually travel through the aggregates, the interfacial zone for these concretes becomes stronger and more homogeneous, and the fracture is trans-granular type. However, in concretes without silica fume, the cracks usually develop around the coarse aggregate resulting in an inter-granular type of fracture.

Acknowledgement

The research reported here was carried out at THD (Technische Hochschule Darmstadt). The second author wishes to acknowledge the financial support from DAAD (Deutscher Akademischer Austauschdienst.)

References

- Bentur, A. (1991) Microstructure of high strength concrete. Darmstädter Massivbau-Seminar, Band 6, IV, 1991, 1-16.
- Gettu, R., Bazant, Z.P. and Karr, M.E. (1990) Fracture properties and brittleness of high strength concrete. **ACI Materials Journal**, 87, 608-618.

- König, G., Bergner, H., Grimm, R. and Simsch, G. (1993) Utilization of high-strength concrete in Europe, in **Utilization of High Strength Concrete**, Vol.1 (eds I.Holand and E.J.Sellevold), Symposium in Lillehammer, Norway, 45-56.
- Mitsui, K., Li, Z., Lange, D.A. and Shah, S.P. (1994) Relationship between microstructure and mechanical properties of the paste-aggregate interface. **ACI Materials Journal**, 91, 30-39.
- Rommel, G. (1992) Tensile and shear behavior of HSC members. PhD Thesis, THD, Darmstadt (in German).
- Sarkar, S.L. (1994) The importance of microstructure in evaluating concrete, in **Advances in Concrete Technology**. (ed V.M. Malhotra), CANMET, Second Edition, Ottawa, 125-160.
- Shah, S.P. (1990) Fracture toughness for high strength concrete. **ACI Materials Journal**, 87, 260-265.
- Skalny, J.P. (ed) (1989) **Material Science of Concrete I**. The American Ceramic Soc. Inc., Westerville, OH.
- Taşdemir, C., Taşdemir, M.A., Lydon, F.D. and Barr, B.I.G. (1994) Influence of microsilica on the strain softening response of concrete, in **Localized Damage III** (eds C.A. Brebbia, M.H. Alidabi, A. Carpinteri, S. Kalisky, and D.J. Cartwright), Computational Mechanics Publications, Southampton, 149-156.
- Taşdemir, C., Sarkar, S.L., Taşdemir, M.A., Akyüz, S. and Koca, C. (1995) Effect of silica fume on the brittleness of high strength concretes under compression, to be submitted at ERMCO 95, Istanbul.
- van Mier, J.G.M. (1991) Mode I fracture of concrete: Discontinuous crack growth and crack interface grain bridging. **Cement and Concrete Research**, 21, 1-15.
- Walraven, J.C. (1991) High strength concrete. **Betonwerk+Fertigteil+Technik**, 6, 45-52.
- Wittmann, F.H. (1983) Structure of concrete with respect to crack formation, in **Fracture Mechanics of Concrete** (ed F.H. Wittmann), Elsevier Applied Science, London, 43-74.